Atmospheric Research 174–175 (2016) 18–30

Contents lists available at ScienceDirect

Atmospheric Research

journal homepage: www.elsevier.com/locate/atmosres

Cloud optical depth from total and UV solar irradiance measurements at two sites of the Atacama Desert in Chile

Eduardo Luccini [a,b,*], Miguel Rivas [c], Elisa Rojas [c]

[a] CONICET - Centro de Excelencia en Productos y Procesos de la Provincia de Córdoba (CEPROCOR). Sede Santa María de Punilla, Pabellón Ceprocor (X5164), Córdoba, Argentina
[b] Facultad de Química e Ingeniería, Pontificia Universidad Católica Argentina. Av. Pellegrini 3314 (2000), Rosario, Santa Fe, Argentina
[c] Laboratorio de Radiación Solar Ultravioleta, Departamento de Física, Facultad de Ciencias, Universidad de Tarapacá, Casilla 7-D, Arica, Chile

ARTICLE INFO

Article history:
Received 4 February 2014
Received in revised form 12 January 2016
Accepted 15 January 2016
Available online 23 January 2016

Keywords:
cloud optical depth
solar irradiance
shortwave
UV
Southeast Pacific
Atacama

ABSTRACT

The visible cloud optical depth (COD) for overcast stratocumulus was estimated at Arica (18.47°S, 70.31°W, 20 m above sea level (asl)) and Poconchile (18.45°S, 70.07°W, 560 m asl), northernmost Chilean sites distant about 30 km in the Atacama Desert, during morning hours for days in which cloudiness dissipates giving cloudless afternoons, from 10 min averaged measurements of total shortwave solar irradiance (ToSI) and ultraviolet solar irradiance (UVSI) during the period 2002–2005. One-dimensional radiative transfer model calculations were made to establish a theoretical relationship between the visible COD, the cloud effective transmittance in both ToSI (CET_{To}) and UVSI (CET_{UV}), and the solar zenith angle (SZA). It is used to estimate COD from the previously measured CET by Luccini et al. (2011). Measurements in both ToSI and UVSI broadband ranges showed to be reliable to determine the visible COD within this frame. Overcast COD at the coastal site of Arica (typical COD ~15) is slightly larger than at the inland site of Poconchile (typical COD ~11). Maximum sensitivity of the retrieved CODs was found to variations in the cloud droplet effective radius, surface albedo and aerosol optical depth in both ranges, and in the total ozone column additionally in UVSI. The obtained CODs are linearly related but are higher compared with those from two other parametric methods using the same data. A simple rational expression of CET as a function of COD enables to estimate a mean (spectral and regional) surface albedo in each range that is in turn applicable to fit appropriately the ratio CET_{To}/CET_{UV}. Instantaneous overpass MODIS-Terra satellite COD at 660 nm show a good agreement with simultaneous (within ±5 min) ground-derived COD at both sites.

1. Introduction

Radiative effects of clouds are determinant to the Earth's climate. In-situ information obtained within the clouds from instruments onboard aircrafts allow direct measurements of cloud microphysical and optical properties, useful to validate locally those parameters retrieved remotely both by satellite or ground instruments (King et al., 1990; Dong et al., 1998; Min et al., 2003). On the other hand, remote information of cloud optical properties by means of passive receptors is obtained basically in two ways, the first from above the clouds by measuring the solar radiation reflected upwards by the clouds, including measurements from instruments onboard satellites (e.g., Rossow and Schiffer, 1991; Barker and Liu, 1995; Loeb and Coakley, 1998; Platnick et al., 2003; Harshvardhan et al., 2004) and onboard aircrafts (e.g., Kuo et al., 1990; Rawlins and Foot, 1990; Barker et al., 2002; King et al., 2004). The second approach is from below the clouds by measuring the solar radiation transmitted by the clouds, considering also the multiple reflections of radiation between the Earth's surface and the clouds. It includes radiometry experiments on aircraft flights below the cloud's base (e.g., Rawlins and Foot, 1990) but, more commonly, it is carried out with solar radiance and/or irradiance, spectral and/or broadband, measurements from ground-based instruments to infer cloud optical properties not only over the continent, but also over the oceans through ship-mounted instruments (e.g., Fitzpatrick and Warren, 2005). Measurements from the surface are also useful as local references to validate satellite retrievals of cloud optical properties (e.g., Min and Harrison, 1996; Li et al., 1999).

The cloud optical depth (COD) is the line integral of the cloud extinction coefficient along the vertical extension of the clouds. It is a key input parameter for any analysis of the atmospheric dynamical-chemical-radiative equilibrium and evolution. Several algorithms were developed to determine the COD from measurements of surface solar

* Corresponding author at: CONICET - Centro de Excelencia en Productos y Procesos de la Provincia de Córdoba (CEPROCOR). Sede Santa María de Punilla, Pabellón Ceprocor (X5164). Tel.: +54 3541 48 9651/53; fax: +54 3541 48 8181.
E-mail addresses: eluccini@ceprocor.uncor.edu, eluccini@ceprocor.uncor.edu (E. Luccini), mrivas@uta.cl, erojas@uta.cl (M. Rivas).

http://dx.doi.org/10.1016/j.atmosres.2016.01.007
0169-8095/

global (direct + diffuse) and diffuse irradiances, using narrowband or broadband radiometers (Leontyeva and Stamnes, 1994; Min and Harrison, 1996, 1998; Boers, 1997; Dong et al., 1997, 1998, 1999; Anikine et al., 1998; Barker et al., 1998; Marshak et al., 2000; Daniel et al., 2002; Dong and Mace, 2003; Barnard and Long, 2004; Min et al., 2004; Rozwadowska, 2004a; Fitzpatrick and Warren, 2005; Qiu, 2006; Matamoros et al., 2011; Yin et al., 2011; Serrano et al., 2013, 2014), needing even complementary measurements of ancillary parameters such as the liquid water path (LWP). Irradiance measurements by total shortwave thermopile sensors require a correction for thermal infrared loss as well (Dutton et al., 2001; Long et al., 2003; Younkin and Long, 2003; Vignola et al., 2007).

The overcast sky cases, especially the stable stratocumulus systems, are particularly appropriate to study given that they can be reliably represented by 1D homogeneous plane-parallel radiative transfer models and the COD depends on very few parameters. In fact, the optical properties of a plane-parallel homogeneous water cloud layer can be characterized through their cloud droplet effective radius (r_e) and their COD, which is in turn proportional to the LWP (Hu and Stamnes, 1993; Leontyeva and Stamnes, 1994). Radiation reflected upwards by the clouds allows retrieving both r_e and COD from satellite or aircraft measurements, by differential absorption between a weakly and a strongly absorbing wavelength. Nevertheless, the radiation transmitted by the clouds is much more sensitive to changes in the COD than to changes in r_e (Leontyeva and Stamnes, 1994), affording the development of simpler algorithms to infer the COD directly from the downward transmitted solar radiation and the solar zenith angle (SZA), once the value of r_e has been defined.

Extensive networks exist around the world measuring broadband total shortwave solar irradiance (ToSI, 300–3000 nm) on a horizontal plane at surface, some of them accompanied by simultaneous measurements of ultraviolet solar irradiance (UVB: 280–315 nm, UVA: 315–400 nm), in general weighted by the erythemal action spectrum of typical human skin (McKinlay and Diffey, 1987) as UVSI in this work, but without diffuse irradiance measurements or complementary instrumentation that would enable the application of sophisticated methods to infer the COD. So, algorithms using only global irradiance measurements are valuable and enhance the possibility to estimate cloud optical properties over large regions. This is the type of algorithm that we employ in the present work. Key parameters in irradiance-based COD retrievals are the cloud effective transmittance (CET, the ratio of the surface irradiance under cloudy conditions to the expected surface irradiance that would be registered for a cloudless sky), SZA, and r_e. The retrieval's accuracy improves substantially if the CET is independent of the absolute calibration of the instrument, that is, when the own instrument's measurements are used to determine the expected clear-sky irradiance for each measurement under cloudy condition. This is the case of the present work, where the COD is estimated from the previously measured CET (Luccini et al., 2011) by linear interpolation within a model-calculated look-up-table relating COD, CET and SZA. The parametric algorithms developed by Fitzpatrick et al. (2004) and Barnard et al. (2008) use basically the same variables to estimate the COD, and we take them as a reference to compare our results. Measurements and radiative transfer model calculations in both ToSI and UVSI ranges were used also by Serrano et al. (2015a) to demonstrate that the COD may be considered spectrally flat between both ranges, and by Serrano et al. (2015b) to correlate COD with different atmospheric transmission factors, namely CET and the clearness index, primarily under cumulus and stratocumulus overcast conditions. Mateos et al. (2014) estimated the COD from ground-based measurements of solar shortwave radiation to evaluate the surface shortwave cloud radiative forcing under overcast conditions.

Major observational campaigns including extensive ship transects are being deployed over the Southeastern Pacific Ocean in order to obtain a wide collection of simultaneous measurements to understand this complex and particular system containing one of the more persistent stratocumulus decks in the world. They include the East Pacific Investigation of Climate (EPIC) (Bretherton et al., 2004; Bigorre et al., 2007), the Pan American Climate Studies (PACS) field experiments Stratus 2003 and Stratus 2004 (Kollias et al., 2004; Serpetzoglou et al., 2008), and the VOCALS program (VAMOS [Variability of American MOnsoon Systems] Ocean-Cloud-Atmosphere-Land Study) (Wood et al., 2011; Mechoso et al., 2014). Several particular features arise from these campaigns and from satellite retrievals over this Pacific region including Arica Bight, such as important zonal/meridional gradients in cloud droplet mean diameter, cloud droplet effective radius, drizzle drop mean size, drizzle drop number concentration, cloud geometric thickness, cloud liquid water path and cloud-top height, below-cloud aerosol number concentration and cloud droplet number concentration, many of them related in part to the intensive sulfur emissions from the major copper smelters in the region (Huneeus et al., 2006; Zuidema et al., 2009; Painemal and Zuidema, 2010; Wood, 2012; Twohy et al., 2013). However, very few reports exist of local in situ measurements over the continental strip of the Atacama Desert (e.g., Chand et al., 2010; Garreaud et al., 2011; Rutllant et al., 2013), as most of the regional studies over the Southeastern Pacific emphasize the marine environment from the coast offshore.

The notable regularity of the Atacama Desert's climate along the West coast of South America enabled to determine CET over this continental region using an empirical method (Luccini et al., 2011). The same data set, consisting in simultaneous 10-min averaged measurements of ToSI and UVSI, together with 1D model irradiance calculations to establish the visible COD as a function of the CET (in both the ToSI and UVSI) and the SZA, are used in this work to estimate the COD at two locations of Northern Chile in the Atacama Desert: the coastal city of Arica and the inland locality of Poconchile. Arica is placed at the open coast in a wide bight, directly connected to the marine stratocumulus deck. On the other hand, Poconchile is located about 30 km inland from the coast on the valley of the small Lluta River, surrounded by deserted low hills being most influenced by continental conditions. The sensitivity to the variation of different parameters and uncertainties involved in the determination of COD are analyzed. The relation between CET and COD is studied in detail. The estimated CODs are also compared with those obtained from two algorithms that parameterize COD as a function of CET and SZA. Simultaneous overpass MODIS Terra satellite-retrieved COD at 660 nm is also compared with the estimated visible COD from the present work at both sites.

2. Methodology

The CET determined previously from simultaneous solar irradiance measurements in the ToSI and UVSI ranges at both locations, Arica and Poconchile, is used in this work as a base to infer the COD for the overcast stratocumulus here considered. The instruments, its measurements and data analysis to determine the CET were described by Luccini et al. (2011), together with the calculations using the Fu-Liou plane-parallel 1D radiative transfer model (Fu and Liou, 1992, 1993; Rose and Charlock, 2002), used here to establish the visible COD as a function of CET in both ranges ToSI (CET_{To}) and UVSI (CET_{UV}) and the SZA. As explained by Luccini et al. (2011), UVA calculations were used in the UVSI range since both UVB and UVIndex outputs are not enough reliable to determine the CET with the Fu-Liou code particularly for large SZA (Su et al., 2005). However, given that changes in the vertical total ozone column (TOC) affect the multiple reflections of UVSI between the top of the cloud and the atmosphere above, and between the bottom of the cloud and the atmosphere/surface below, UVIndex outputs will be used from Fu-Liou code only at a fixed SZA to analyze the sensitivity of the inferred CODs to the TOC in Section 3.2. Broadband downwelling irradiance calculations at the surface under homogeneous overcast sky were made for COD equal to 5, 10, 15, 20, 25, 30, 40, 50, 60, 70, 80, 90 and 100, and for 0°-90° SZA range. COD was set to 0 for the clear-sky case. Best estimated values of the input parameters are (Luccini et al.,

2011): a homogeneous infinite plane-parallel cloud layer of 400 m thickness with cloud base at 900 m asl and cloud top at 1300 m asl, cloud droplet effective radius $r_e = 8$ μm, TOC of 270 DU, continental aerosol type with an optical depth of 0.3 at 550 nm and a broadband surface albedo of 0.10. Afterwards, the modeled CET was determined for each modeled COD value as the ratio of the cloudy-sky over the clear-sky cases in both ToSI and UVSI ranges and as a function of the SZA. Fig. 1 shows the modeled CET in the ToSI and UVSI as a function of the SZA for the whole range of calculated visible CODs. In mathematical terms it can be observed from Fig. 1 that, for a fixed SZA, a biunivocal curve links the modeled COD and CET, making possible to construct look-up-tables in the ToSI and UVSI to obtain COD by interpolation from each measured value of CET at its given SZA. Precisely, the measured CET points for cloudy cases, corresponding to CET < 0.80 in both ranges, are also shown in Fig. 1 as obtained by Luccini et al. (2011). Given that clouds affect more strongly the ToSI than the UVSI for both the attenuation (particularly for overcast cases) and the enhancing (due to broken clouds) at ground (Cede et al., 2002; Calbó et al., 2005; Antón et al., 2011), the additional condition $CET_{To} < CET_{UV}$ was imposed to the measured data in order to assure that they belong mostly to overcast cases. Situations with CET > 0.80 correspond to COD <5 and they were analyzed in detail by Luccini et al. (2011). Barnard et al. (2008) use exactly the same threshold CET = 0.80 to distinguish optically thick (COD >5) from optically thin (COD <5) clouds under overcast sky, the last considered directly as cirrus clouds. In turn, Boers et al. (2000) had determined an increase in the uncertainty for the estimation of CODs <5 in pyranometer-based algorithms even for overcast sky cases.

3. Results and discussion

3.1. Effective COD at Arica and Poconchile

Fig. 2 shows the normalized histograms of COD obtained from the measured CET of Fig. 1 in the ToSI range (COD_{To}) and in the UVSI range (COD_{UV}). We emphasize that the denominations COD_{To} and COD_{UV} are only to distinguish the measurement broadband range from which the same parameter is inferred: the visible COD. The maximums of these distributions were obtained with smoothing curves and are also denoted in Fig. 2. They characterize the visible COD for overcast stratocumulus and correspond to COD_{To} ~ 13 (11) and COD_{UV} ~ 16 (12) at Arica (Poconchile), i.e. COD is generally slightly larger at Arica than at Poconchile. Luccini et al. (2011) pointed out that the minimum CET observed in Fig. 1 imply a limit to the maximum COD registered over this region, fact that is confirmed now in Fig. 2 since CODs larger than ~60 are certainly uncommon due to the predominance of stratocumulus-type clouds, as the climatic conditions of the region prevent the formation of convective clouds typical of the surrounding Tropical regions (e.g., Garreaud and Wallace, 1997). Compared with the regular stratocumulus system in the Northern Pacific, the obtained COD values are similar (Nakajima et al., 1991; Szczodrak et al., 2001), and also with overcast stratocumulus over the Baltic Sea (Rozwadowska, 2004a). Nevertheless, the strong gradients observed in the cloud parameters from the coast offshore in regions with regular stratocumulus systems around the world (Zhang et al., 2010; Wood, 2012) difficult the comparison between values registered over open ocean and those over coastal or inland sites, even within this enclosed Pacific region.

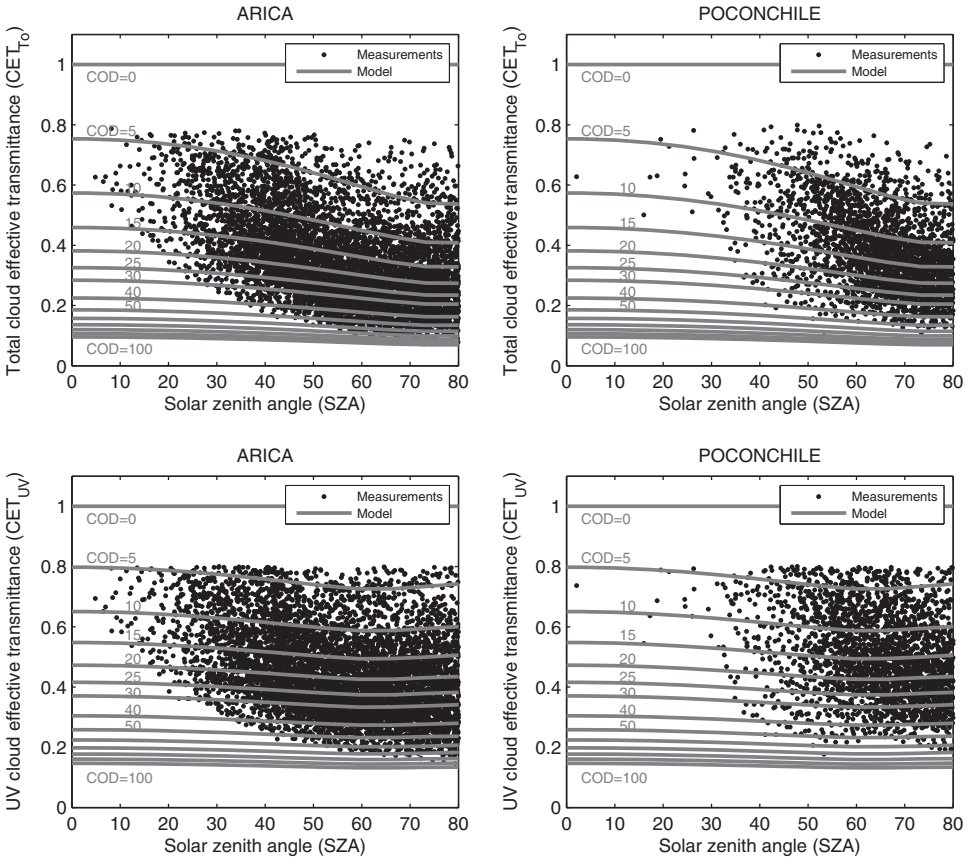

Fig. 1. Measured cloud effective transmittance (CET) for mostly overcast-sky conditions ($CET_{To} < 0.80$, $CET_{UV} < 0.80$ and $CET_{To} < CET_{UV}$) from the work by Luccini et al. (2011) in the total shortwave range (top) and in the UV range (bottom) as a function of the solar zenith angle (SZA) at Arica (left) and at Poconchile (right). Gray lines represent the modeled CET in both ranges as a function of SZA for visible cloud optical depth (COD) from 0 (clear-sky case) to 100. Only data for SZA < 80° were selected to avoid the larger uncertainties. COD is determined in the present work for each CET measured point at its corresponding SZA, by linear interpolation within the model-calculated COD-CET-SZA look-up-table.

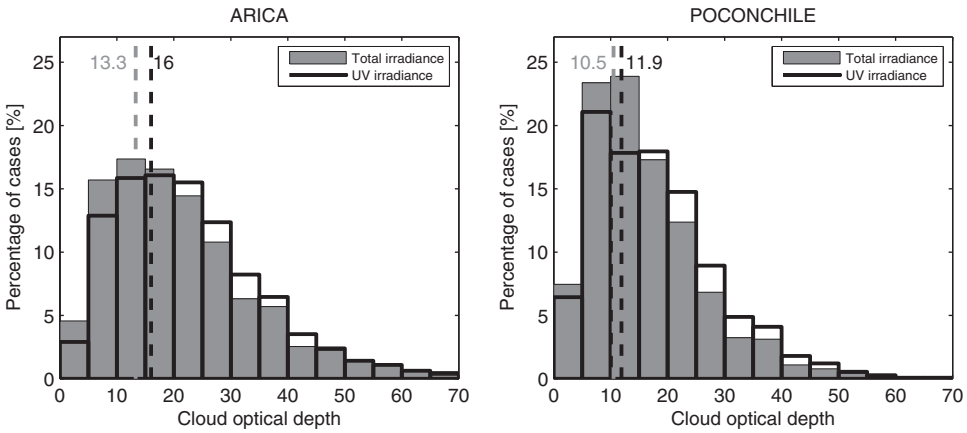

Fig. 2. Normalized histograms of the visible cloud optical depth (COD) determined from the CET measured points of Fig. 1 in the total shortwave range (gray shaded bars) and in the UV range (black contour bars) through the model-calculated COD-CET-SZA look-up-table at Arica (left) and Poconchile (right). Dashed lines denote the maximum of the distributions determined from smoothing curves in the total shortwave (gray) and UV (black) ranges. Their values characterize the COD for overcast-sky conditions at each site.

COD_{To} and COD_{UV} closely agree, with COD_{UV} slightly larger than COD_{To} on average at both sites as it can be observed in Fig. 3 (top). Linear fit parameters are presented in Table 1, and the possible causes of the differences will be analyzed in Section 3.2. Using the parameterization by Fitzpatrick et al. (2004) (FBW, as will be described in Section 3.3) a very similar result is observed also in Fig. 3 (bottom). Particularly, it can be noted that the agreement is very good on average using both algorithms for CODs ranging between 10 and 20 that are predominant in this region (see Fig. 2). So the irradiance measurements in both broadband ranges, ToSI and UVSI, have shown to be reliable for estimating de visible COD through this type of algorithms.

In Fig. 4 it can be observed that CET has a strong inversely proportional relation with COD, the most important parameter influencing CET together with the SZA. Relations of Fig. 4 in the UV range closely agree with those modeled by Antón et al. (2012), although in our case we have not independent values to compare, as CODs are determined from the model calculations itself. Given the sharp observed correlation between CET and COD for data in the range $0 < SZA < 80°$, the measured

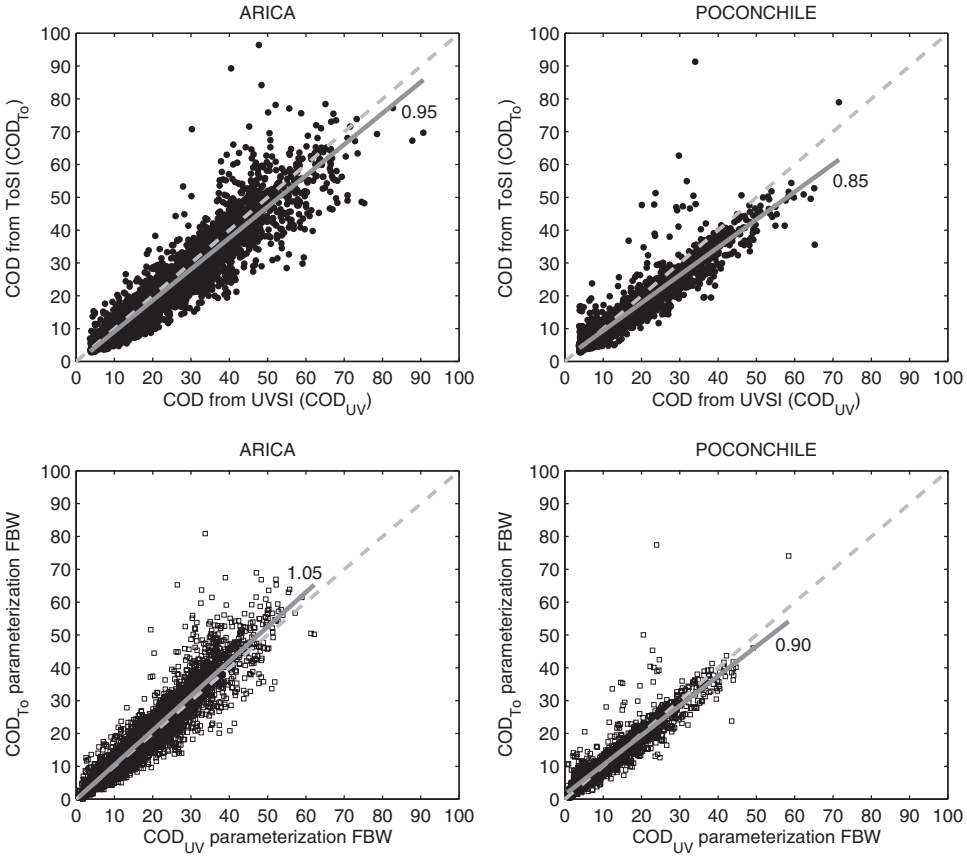

Fig. 3. Relation between the visible cloud optical depth determined from the total shortwave range (COD_{To}) and the visible cloud optical depth determined simultaneously from the UV range (COD_{UV}) in the present work (top) and from the FBW parameterization (Fitzpatrick et al., 2004) (bottom) at Arica (left) and at Poconchile (right). Numbers within the figures are the slopes of the corresponding dark-gray linear fit curves, whose parameters are summarized in Table 1. Dashed light-gray lines are for reference with slope = 1.

Table 1
Values of the slope, square of correlation coefficient (R^2) and root-mean-square-error (RMSE) of the linear fitting curves to correlated COD data at Arica and Poconchile from Figs. 3, 8 and 9.

Figure number	Plotted parameters[a]	Arica				Poconchile			
		Number of data	Slope	R^2	RMSE	Number of data	Slope	R^2	RMSE
Fig. 3	COD_{To}(PW) vs COD_{UV}(PW)	6050	0.95	0.895	4.2	2562	0.85	0.872	3.5
Fig. 3	COD_{To}(FBW) vs COD_{UV}(FBW)	6050	1.05	0.891	3.6	2562	0.90	0.865	2.8
Fig. 8	COD_{To}(PW) vs COD_{To}(FBW)	6050	1.18	0.970	2.2	2562	1.22	0.962	1.9
Fig. 8	COD_{To}(PW) vs COD_{To}(B08)	6050	1.07	0.990	1.3	2562	1.11	0.982	1.3
Fig. 8	COD_{UV}(PW) vs COD_{UV}(FBW)	6050	1.31	0.972	2.2	2562	1.32	0.970	1.9
Fig. 9	MODIS COD vs COD_{To}	150	0.73	0.661	4.7	12	1.34	0.500	8.1
Fig. 9	MODIS COD vs COD_{UV}	150	0.71	0.651	4.8	12	0.79	0.417	8.7

[a] COD_{To}: visible COD estimated from ToSI; COD_{UV}: visible COD estimated from UVSI; PW: present work; FBW: parameterization by Fitzpatrick et al. (2004); B08: parameterization by Barnard et al. (2008); MODIS COD: MODIS-Terra satellite COD at 660 nm.

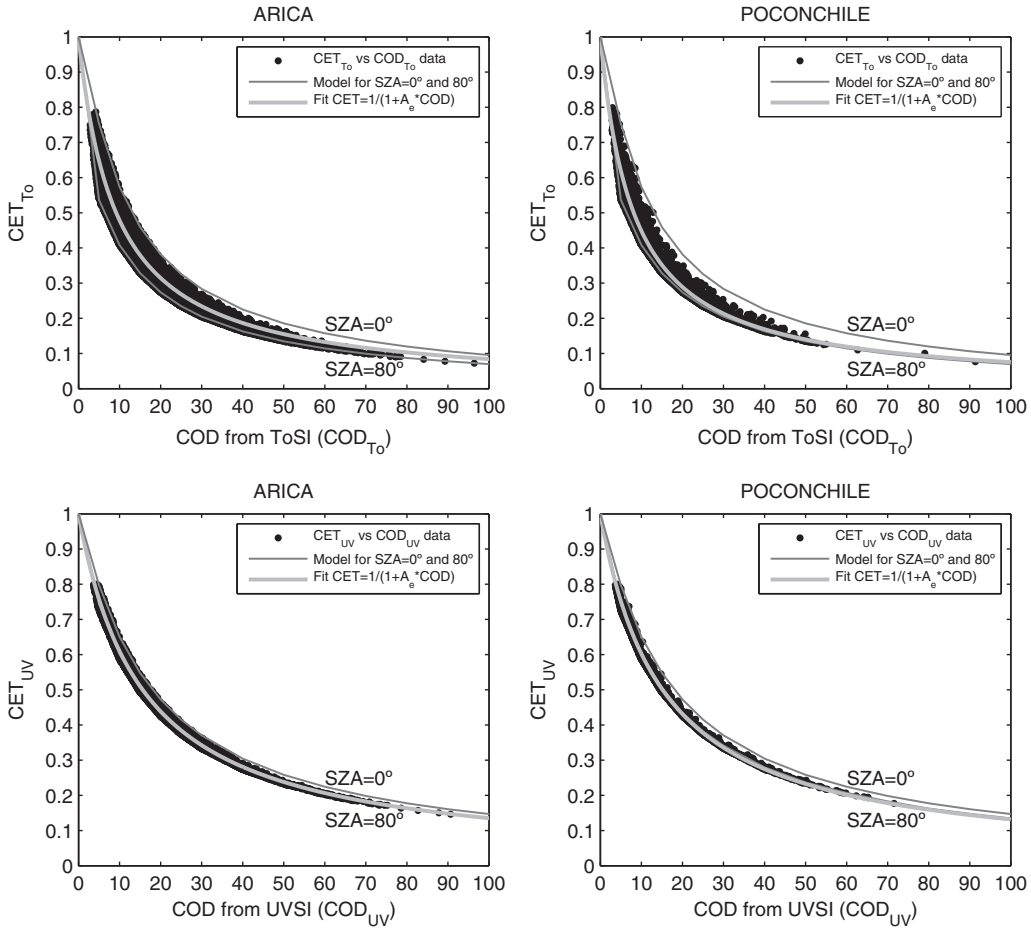

Fig. 4. Measured cloud effective transmittance in the total shortwave range (CET_{To}) (top) and in the UV range (CET_{UV}) (bottom) as a function of the visible cloud optical depth (COD) estimated from the same wavelength range for mostly overcast-sky conditions ($CET_{To} < 0.80$, $CET_{UV} < 0.80$ and $CET_{To} < CET_{UV}$) at Arica (left) and at Poconchile (right). Dark-gray lines represent the modeled CET in each range as a function of the COD for solar zenith angles (SZA) of 0° and 80°. Light-gray line represent fitting curves with the equation $CET = 1/(1 + A_e{*}COD)$. Values of the fitting parameters are $A_{eTo} = 0.109$ (0.123) for ToSI and $A_{eUV} = 0.064$ (0.066) for UVSI at Arica (Poconchile).

points were fitted through the simplest rational expression for CET as a function only of COD, i.e. averaging over the whole range of SZA, constrained to the condition that CET = 1 for COD = 0, with a phenomenological base that was discussed in detail by Fitzpatrick et al. (2004). The equation is:

$$CET = \frac{1}{1 + A_e * COD} \quad (1)$$

where A_e is a fitting parameter that can be considered an estimator of the average surface albedo in ToSI or UVSI. As can be seen in Fig. 4, Eq. 1 provides excellent fits to the data. A_e takes values of 0.109 (0.123) with R^2 = 0.942 (0.958) for ToSI and 0.064 (0.066) with R^2 = 0.994 (0.997) for UVSI at Arica (Poconchile). This is an interesting result for several reasons. Recent spectral surface albedo studies by Varotsos et al. (2014) reported similar average UV albedo values of about 0.10 over open water and over desert sand but, while the albedo decreases progressively for open water towards longer wavelengths, it increases significantly for desert sand. Then, as a regional average for sites placed in an extensive desert with an adjacent open ocean, our reported smaller values of UVSI average surface albedo than ToSI average surface albedo of Fig. 4 are consistent with the results by Varotsos et al. (2014), and they may be considered as a phenomenological correction to the flat surface albedo of 0.10 used in the model calculations. Secondly, the fits obtained with Eq. 1 provide an immediate and consistent fit to the ratio CET_{To}/CET_{UV} as a function of COD, plotted in Fig. 5, at both sites in the form:

$$\frac{CET_{To}}{CET_{UV}} = \frac{1 + A_{eUV} * COD}{1 + A_{eTo} * COD} \quad (2)$$

where A_{eTo} and A_{eUV} are the estimated mean values of surface albedo in ToSI and UVSI respectively at each site. As expected for this case of overcast sky, the ratio CET_{To}/CET_{UV} decreases progressively with increasing COD, due to the known fact that cloudiness attenuates more effectively the ToSI than the UVSI at ground. In principle, Eq. 2 could be used as a broad estimator of the ratio CET_{To}/CET_{UV} for overcast cloudiness (at least homogeneous stratocumulus cases) at other places where the mean A_{eTo} being higher than A_{eUV}. It can be noted from Figs. 4 and 5 that the fitting curves at Poconchile are closer to the model curves for SZA = 80°, since cloudiness dissipates earlier during the morning than at Arica and most of points at Poconchile correspond to larger SZA (see Fig. 1).

In order to test the consistency of the CODs obtained from different wavelength ranges, CET_{To} (CET_{UV}) was plotted as a function of the cloud optical depth inferred from the other broadband range, COD_{UV} (COD_{To}) in Fig. 6. Beyond the expected larger scatter in the data of Fig. 6, the average curves obtained through a moving window from data of Figs. 4 and 6, plotted both in Fig. 6, differ by less than 10% for CODs <60, showing the reliability of the algorithm to estimate the visible COD from both ToSI and UVSI measurements.

3.2. Precision and involved uncertainties

To assess the incidence of variations in the model input parameters on the retrieved CODs, a sensitivity study was made in ToSI and UVSI (in UVA range except for TOC where calculations were made in UVIndex range) for SZA = 60° where most of overcast sky points are registered (see Fig. 1), centered at COD = 15 that is a typical value over the region (see Fig. 2), covering the principal variables entering the calculations: cloud droplet effective radius (r_e), cloud geometrical thickness (*CGT*), total ozone column (*TOC*), aerosol optical depth (*AOD*), surface albedo (*A*) and surface elevation (*SE*). Then, calculations to determine CET at a constant value of COD equal to 10, 15 and 20 were made for r_e = 5 μm and 11 μm, *CGT* = 200 m with cloud base at 1000 m and cloud top at 1200 m, *CGT* = 600 m with cloud base at 800 m and cloud top at 1400 m, *TOC* = 220 DU and 320 DU, *AOD* = 0 and 0.6, *A* = 0 and 0.2 and *SE* = 600 m asl (about the altitude of Poconchile), maintaining fixed in each case all the remaining parameters at their reference values (see Section 2): r_e = 8 μm, *CGT* = 400 m (cloud base at 900 m and cloud top at 1300 m), *TOC* = 270 DU, *AOD* = 0.3, *A* = 0.10 and *SE* = 0 m asl. Calculations compared with the reference are displayed graphically in Fig. 7 (left). However, CET must be considered the fixed parameter to fit by the calculations as it was previously determined from irradiance measurements. Then, variations in the inferred COD due to changes in the model parameters must be analyzed at constant CET instead at constant COD, from the reference COD = 15. The methodology for the analysis at constant CET is explained in Fig. 7 (right). Table 2 shows the percentage change affecting the retrieved COD at constant CET in each case. Physically, the results of Fig. 7 and Table 2 indicate that, when the variation of a given parameter would imply an increment of CET at constant COD (either by relative increment of the irradiance under cloudy conditions in the numerator or by relative decrease of the clear-sky irradiance in the denominator), the COD must in fact be increased to maintain as a constant the value of CET. Variations in r_e, *AOD* and *A* have the largest influence on the estimation of COD, with their values higher than the references implying that the present CODs are underestimated. Fitzpatrick et al. (2004) found a similar dependence of COD on r_e within a wide range of values of SZA and surface albedo. As expected, *TOC* changes have a negligible impact on the estimation of COD_{To}, but instead they influence in a larger extension the estimation of COD_{UV}, although extreme values of 220 DU (the threshold of

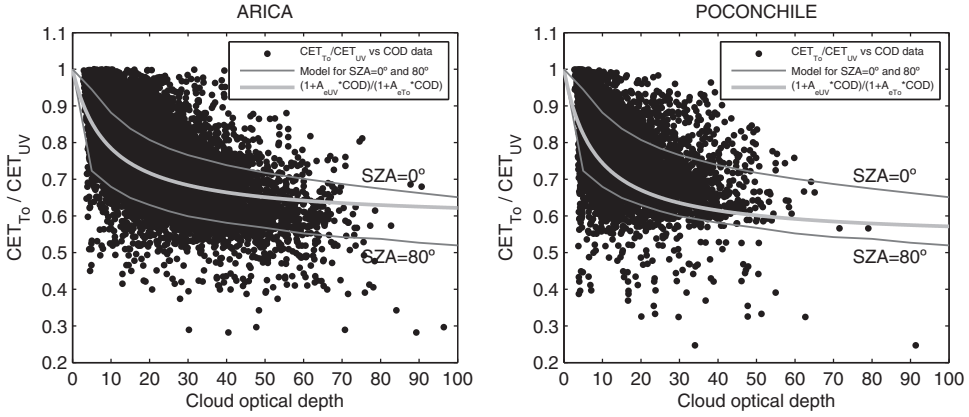

Fig. 5. Ratio of the cloud effective transmittance in the total shortwave range (CET_{To}) to the cloud effective transmittance in the UV range (CET_{UV}) as a function of the visible cloud optical depth (COD) estimated from both ToSI and UVSI for mostly overcast-sky conditions ($CET_{To} < 0.80$, $CET_{UV} < 0.80$ and $CET_{To} < CET_{UV}$) at Arica (left) and at Poconchile (right). Upper and lower dark-gray lines represent the model-calculated ratios for SZA = 0° and 80° respectively. Light-gray fitting line uses the ratio of the fittings to data of Fig. 4 through Eq. 1 in ToSI and UVSI.

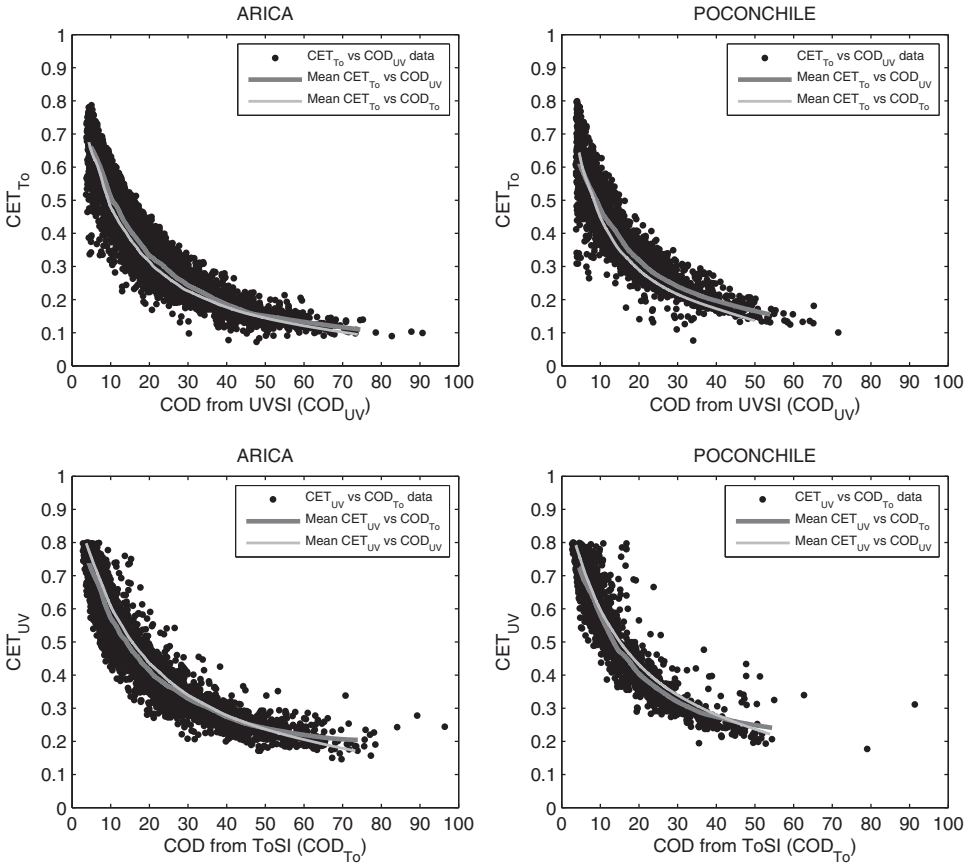

Fig. 6. Measured cloud effective transmittance in the total shortwave range (CET_{To}) (top) and in the UV range (CET_{UV}) (bottom) as a function of the visible cloud optical depth estimated from the UV range (COD_{UV}) (top) and from the total shortwave range (COD_{To}) (bottom) for mostly overcast-sky conditions ($CET_{To} < 0.80$, $CET_{UV} < 0.80$ and $CET_{To} < CET_{UV}$) at Arica (left) and at Poconchile (right). Dark-gray lines represent a moving mean average to the measured data. Light-gray lines represent a moving mean average to the measured data of Fig. 4, in which the plotted CET and COD correspond to the same wavelength range.

ozone "hole" conditions) and 320 DU are infrequent at tropical latitudes taking into account that, for example, the average *TOC* for the period 2004–2010 in the latitudinal band 15°S - 20°S is 257 ± 8 DU (Ziemke et al., 2011). Calculation for SE = 600 m indicates that the present CODs at Poconchile may be slightly overestimated due to the altitude of the site, and changes in *CGT* have a negligible effect on the retrieved CODs at both sites. Worse cases, although improbable, of simultaneous very small (large) actual values of r_e, *A*, *AOD* and large (small) *TOC* would imply that the retrieved COD_{To} are overestimated (underestimated) by a relative bias of about 25% and COD_{UV} by about 30%.

Other sources of systematic bias to be considered in our work are:

- The inhomogeneities of the overcast cloud field. An intrinsic characteristic of every real cloud field is their spatial and temporal variability, even though our case of overcast stratocumulus is probably the closer to the homogeneity of the plane-parallel model simulations (Luccini et al., 2011). The non-linear relation between the irradiance and the COD causes a systematic bias in every method to obtain COD based on solar irradiance averages. As example, a simple calculation with the direct irradiance shows that the COD obtained from the averages of transmitted direct solar irradiance under overcast variable conditions will always underestimate the average of "true" CODs for the same group of measurements. The effect is also valid for the reflected irradiance, and satellite-retrieved COD generally underestimate the true average COD (Kokhanovsky, 2003; Zinner and Mayer, 2006). Boers et al. (2000) and Rozwadowska (2004b) have quantified that the bias in the estimated CODs through pyranometric measurements of solar irradiance at surface due to cloud field inhomogeneities ranges between +1% and −20%, the last case for optically thick and variable clouds, long-term irradiance averages of around 1 h and clouds with high-altitude base. The vertical distribution of drops within the clouds have a smaller impact in the model representation of the clouds (e.g., Evans and Puckrin, 1996), and the Mie resonant absorption of solar radiation within cloud droplets is only relevant in specific narrow spectral bands (Zender and Talamantes, 2006) although its incidence on broadband ranges is negligible.
- The thermal offset by infrared cooling of thermopile pyranometers measuring ToSI produces slightly overestimated values of CET_{To} (Luccini et al., 2011). As can be deducted from Fig. 1 at a fixed SZA, an overestimated CET_{To} causes an underestimated COD_{To}. This effect is not present in the UVSI case given that UV biometers don't suffer infrared cooling. Looking at Fig. 3 (top), this seems to be reflected in the higher values of COD_{UV} than COD_{To} on average. However, this is not verified using the parameterization by Fitzpatrick et al. (2004) at Arica (Fig. 3, bottom left), showing that eventually this effect has a minor consequence on the results.
- Asymmetries in the atmospheric parameters between the morning and the afternoon. Given that afternoon measurements are taken as the expected clear-sky irradiance during the morning and of course ozone, aerosols, and other atmospheric constituents change in time in a continuous way, there is an unavoidable second-order error when their values are considered constant during each day, but this is a generalized assumption in this type of studies and our method has in turn the advantage that it allows to determine the measured CETs regardless of the value of these parameters, as only the assumption that they were constant during the day is necessary

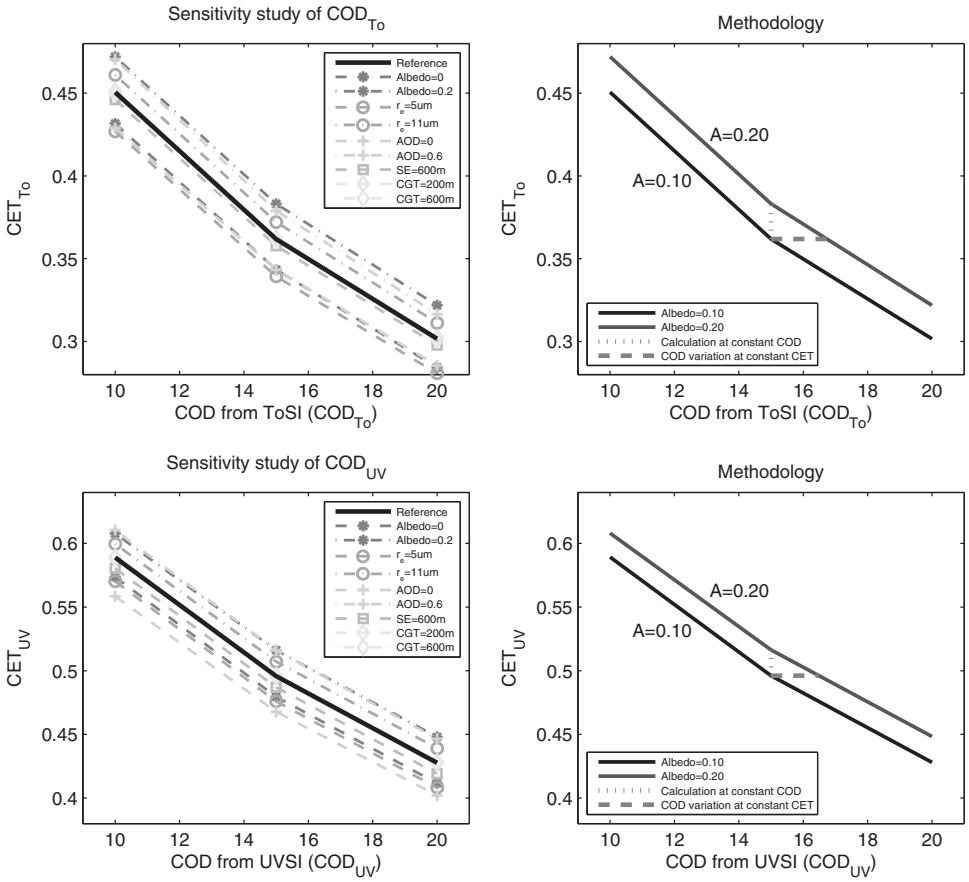

Fig. 7. (left) Sensitivity study to determine the visible cloud optical depth (COD) at SZA = 60° from a reference value of COD = 15 to changes in the principal related parameters: cloud droplet effective radius (r_e), surface albedo (A), aerosol optical depth (AOD), surface elevation (SE) and cloud geometrical thickness (CGT). Sensitivity to the total ozone column (TOC) from Fu-Liou model, UVIndex output, are presented in Table 2. (top) COD determined from the total shortwave range (COD_{To}) and (bottom) COD determined from the UV range (COD_{UV}). (right) Methodology to determine the COD variation at constant cloud effective transmittance (CET) (given that calculations are made at constant COD), using as example the surface albedo variation.

(Luccini et al., 2011). For example, in our case an asymmetry causing a second-order systematic error may be mentioned with respect to the surface albedo: in the afternoons the sun is towards the West over the ocean as seen from ground, and the directional reflectance of the ocean (Li and Garand, 1994), particularly for SZA > 60°, increases the albedo and then the clear-sky reference in an effect that would not be present if morning clear-sky measurements were available when the sun is at the East over the desert, whose albedo is roughly Lambertian (Li and Garand, 1994). Seen at Fig. 1, the underestimated CET caused for this effect gives as result slightly

Table 2
Sensitivity study of the estimated cloud optical depth (COD) to changes in the principal related parameters, modeled at constant cloud effective transmittance (CET) as explained in Fig. 7. Reference calculations were made for COD = 15 and SZA = 60°.

Changed parameter	Reference value	Tested values	Percentage change in COD respect to COD = 15 at constant CET [%][a]	
			COD_{To}	COD_{UV}
Cloud droplet equivalent radius (r_e)	8 μm	5 μm	−8.6	−7.0
		11 μm	5.6	5.6
Surface albedo (A)	0.10	0.0	-7.0	-5.8
		0.20	11.6	9.9
Aerosol optical depth (AOD) at 550 nm	0.3	0	-7.2	-10.3
		0.6	9.1	9.7
Total ozone column (TOC)[b]	270 DU	220 DU	0.14	6.5
		320 DU	-0.08	-5.0
Surface elevation (SE)	0 m (sea level)	600 m asl	−1.5	−3.1
Cloud geometrical thickness (CGT)	400 m (base: 900 m, top: 1300 m)	200 m (base: 1000 m, top: 1200 m)	0.36	0.06
		600 m (base: 800 m, top: 1400 m)	-0.23	-0.06

[a] COD_{To}: visible COD estimated from ToSI; COD_{UV}: visible COD estimated from UVSI.
[b] From Fu-Liou model, UVIndex output.

overestimated CODs, precisely within the range of large SZAs when most of overcast data are registered.

3.3. Comparison with parameterizations of COD

COD is directly interpolated in this work from explicit calculations in the ToSI and UVSI ranges as a function of CET and SZA, once appropriate values of the model input variables have been defined. To facilitate their use for other works, both look-up-tables are available as supplementary material to this manuscript. Our results are compared with the wavelength-independent (in the geometric-optics limit) COD obtained from two parameterizations where CET and SZA are key parameters.

Barnard et al. (2008), hereinafter the B08 parameterization, established the following semi-empirical relation to determine COD using ToSI measurements under overcast sky:

$$COD_{To}^{B08} = \frac{\frac{1.16}{r} - 1}{(1-A)(1-g)} \tag{3}$$

where $r = \frac{CET_{To}}{\sqrt[4]{\cos(SZA)}}$, g is the asymmetry factor of cloud droplets with a recommended value of 0.87 for water clouds as in the present case, and $A = 0.10$ as in our calculations.

Based on spectral model calculations for cases of snow, ice and water surfaces, Fitzpatrick et al. (2004), hereinafter FBW, established a parameterization in ToSI and nine monochromatic wavelengths in such way that COD can be inferred as:

$$COD^{FBW} = \frac{\frac{a + b * \cos(SZA)}{CET}}{c - d * A} - 1 \tag{4}$$

Parameters a and b reach an asymptotic value for COD > 5, so that they can be considered constants to the purposes of this work. Using $r_e = 8.6$ μm, similar to the $r_e = 8$ μm of the present work, the values of parameters defined by Fitzpatrick et al. (2004) are $a = 0.58$, $b = 0.74$, $c = 0.1365$ and $d = 0.1291$ for ToSI and $a = 0.78$, $b = 0.31$, $c = 0.0835$ and $d = 0.0759$ for UV at 370 nm, which are taken as representative of the UVSI range. This formula is applied to estimate COD from both ToSI and UVSI measurements using again $A = 0.10$.

Fig. 8 shows that the CODs obtained from both ToSI and UVSI in the present work have a strong linear correlation with the CODs from both parameterizations and are larger, COD_{To} by a systematic relative bias of about 7% (11%) with respect to the B08 parameterization and of 18% (22%) with respect to the FBW parameterization at Arica (Poconchile), while COD_{UV} by 31% (32%) with respect to the FBW parameterization at Arica (Poconchile). Correlation and linear fit parameters are presented in Table 1. We have tested also the Barnard and Long (2004) parameterization which employs the diffuse total shortwave irradiance instead of the global total shortwave irradiance. Considering our case of overcast stratocumulus with dense water clouds when the solar disc is not visible, it can be assumed that the whole global irradiance in the ToSI range corresponds to the diffuse component (e.g., Harrison

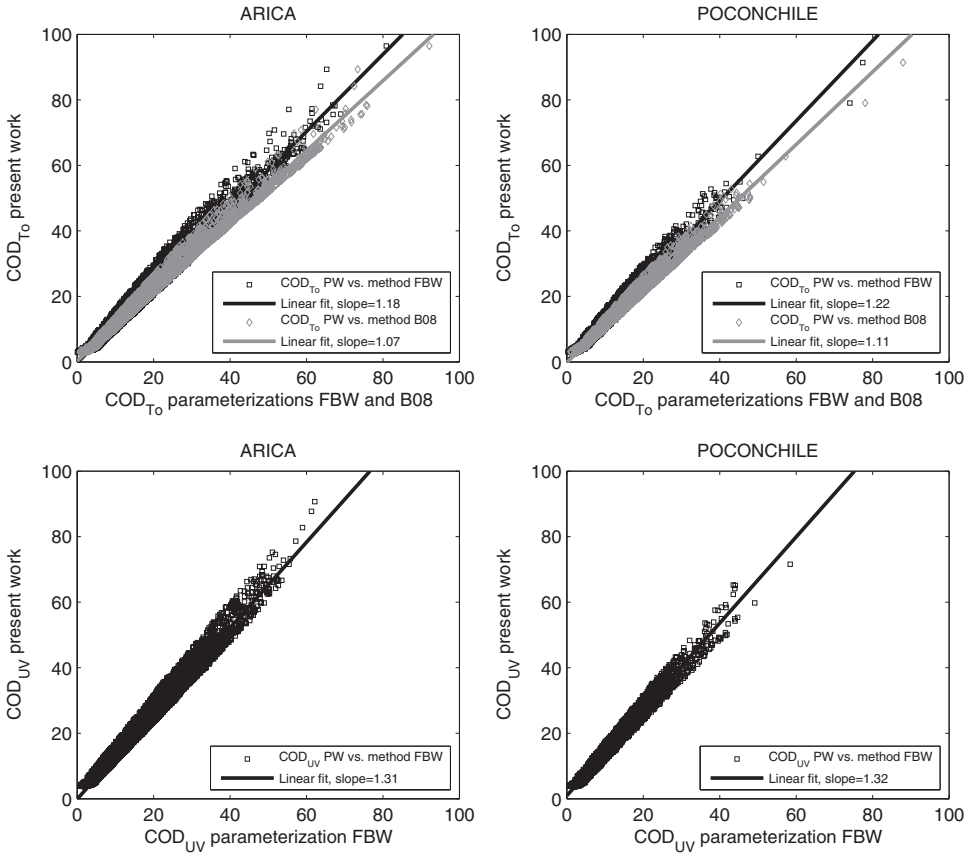

Fig. 8. Comparison between the cloud optical depth (COD) obtained in the present work (PW) at Arica (left) and at Poconchile (right) with the COD obtained from other algorithms using also the measured CET and the SZA. (top) Total shortwave solar irradiance (COD_{To}): parameterizations FBW (Fitzpatrick et al., 2004) (black squares) and B08 (Barnard et al., 2008) (gray diamonds). (bottom) UV solar irradiance (COD_{UV}): only parameterization FBW (black squares). Black and gray solid lines represent a linear fit to the corresponding data, whose parameters are summarized in Table 1.

et al., 2008), and the results with the Barnard and Long (2004) parameterization were in fact very similar to those with the B08 parameterization: COD_{To} from the present work is larger by about 6% (9%) with respect to Barnard and Long (2004) parameterization at Arica (Poconchile).

3.4. Comparison with MODIS satellite data

Narrowband COD at 660 nm is one of the products of the Moderate Resolution Imaging Spectroradiometer (MODIS) instruments aboard Terra Earth Observing System AM and Aqua Earth Observing System PM satellites (King et al., 1998). Terra satellite passes from north to south across the equator in the local morning, between 10:00 and 12:00 LT, simultaneously with our ground-estimated CODs and then the MODIS Terra Level 2 Cloud product data (MOD06_L2 Joint Atmosphere Product ATM L2, NASA Goddard Space Flight Center) are used for comparison. In turn, Aqua satellite passes south to north over the equator in the local afternoon and their data are not useful for this purpose, as our work consists only of morning COD data. Given that ground-estimated COD are determined every 10-min, they are compared with an instantaneous overpass satellite data within a difference of ±5 min. Required conditions for the comparison are mostly overcast sky conditions ($CET_{To} < 0.80$, $CET_{UV} < 0.80$ and $CET_{To} < CET_{UV}$) for the ground-estimated COD, MODIS cloud fraction larger than 0.9, and satellite data within a radius of 20 km of each site. Results are shown in Fig. 9 where MODIS COD is compared with both COD_{To} and COD_{UV} which refer to the same parameter: the ground-estimated visible COD. It can be noted in Fig. 9 that most of points correspond to distances of less than 10 km from each site (solid black dots), and only a few to distances between 10 and 20 km (contoured black dots). As deducted from Fig. 1, cloudiness dissipates earlier over Poconchile than over Arica, and for this reason there are much more simultaneous satellite (overpass at 10–12 LT) and ground data to compare at Arica. Correlation and linear fit parameters are presented in Table 1. The reduced number of data at Poconchile, their scarce correlation and large root-mean-square-error makes their analysis statistically non-significant, and the analysis will be centered on the comparison at Arica. Taking into account that the comparison implies almost instantaneous data obtained remotely through radiative information from the opposite sides of the cloud deck, the agreement between the satellite-retrieved and the ground-estimated COD may be considered as good at Arica for both sources of ground-estimated COD: the ToSI and UVSI measurements. Again, it can be noted that the agreement is very good on average at Arica for CODs ranging between 10 and 20 that are predominant in the region (see Fig. 2). Comparison at Arica shows the same behavior than that reported by Li et al. (2014): MODIS-retrieved CODs are smaller than the ground-retrieved CODs, particularly for COD > ~ 30, and their difference enhances for increasing CODs. Li et al. (2014) relate this behavior to the effect of dense absorbing surface aerosol loads influencing the ground-based retrievals but not the satellite retrievals, which is a plausible

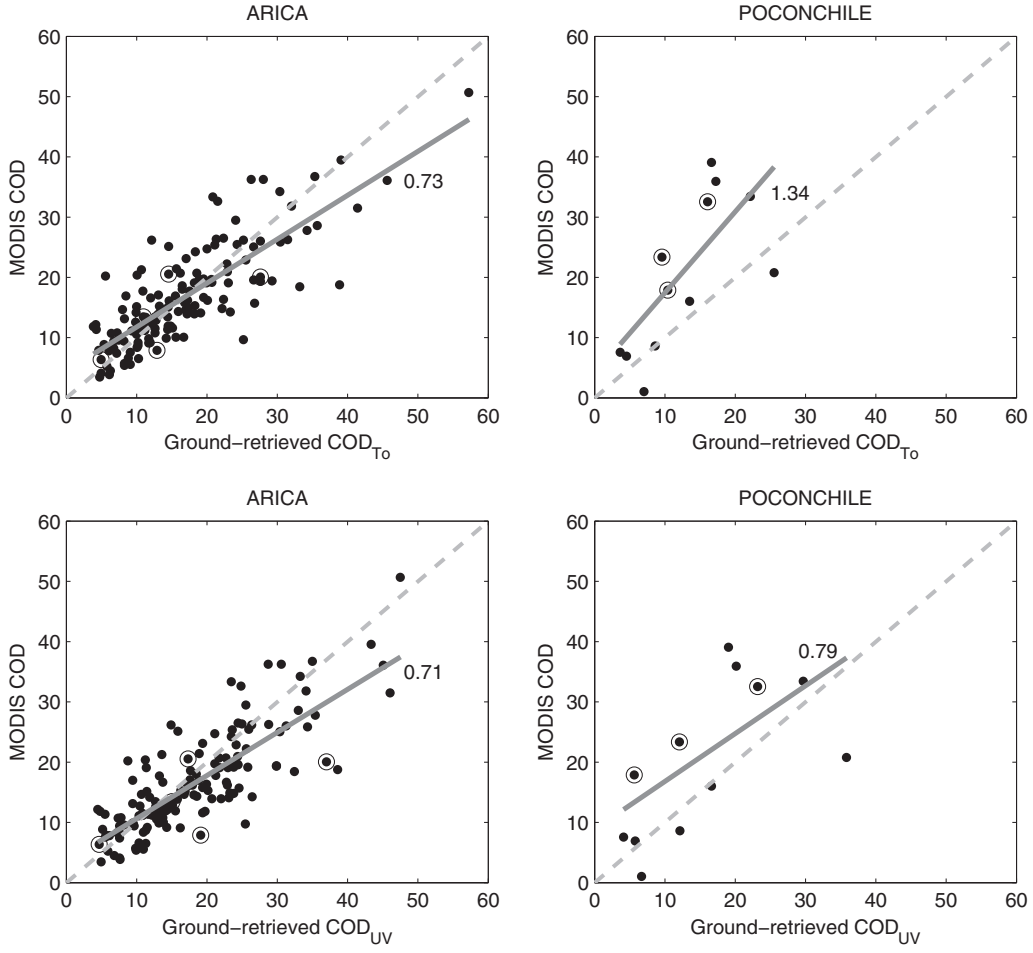

Fig. 9. Comparison between simultaneous (within ±5 min) overpass overcast-sky (cloud fraction larger than 0.9) satellite MODIS-Terra cloud optical depth at 660 nm and the ground-retrieved visible cloud optical depth estimated in the present work from the total shortwave range (COD_{To}) (top) and from the UV range (COD_{UV}) (bottom) at Arica (left) and at Poconchile (right). Solid black dots correspond to a distance shorter than 10 km from MODIS data to each site, while contoured black dots correspond to a distance between 10 km and 20 km. Numbers within the figures are the slopes of the corresponding dark-gray linear fit curves, whose parameters are summarized in Table 1. Dashed light-gray lines are for reference with slope = 1.

argument also over the Atacama desert strip whose stable high aerosol content often registers values quite larger than the $AOD = 0.3$ used in this work (Otero et al., 2006; Eck et al., 2012). In those cases, ground-retrieved CODs would be underestimated (see Section 3.2), so that the differences between MODIS CODs and the "actual" ground-based CODs would be even larger for COD > ~30, in close agreement with the analysis by Li et al. (2014). Even though both natural and anthropogenic aerosols over the Arica region are predominantly non-absorbing (Eck et al., 2012), the effect is attributed to the high values of *AOD* regardless of the aerosols' composition. In turn, for COD < ~20, Painemal and Zuidema (2011) and King et al. (2013) report slightly larger MODIS COD versus aircraft in situ COD measurements over the surrounding Southeast Pacific ocean, which basically agrees with our results over Arica shown in Fig. 9. Eventually, this behavior towards the smaller CODs may be caused by thin high-altitude clouds which are more easily detectable by the satellite. As a reference, comparison of MODIS-retrieved CODs with ground-estimated CODs from the FBW and B08 parameterizations present the same qualitative behavior, with slopes of 0.82 (1.45) in COD_{To} and 0.88 (0.96) in COD_{UV} with respect to the FBW parameterization, and 0.77 (1.49) in COD_{To} with respect to the B08 parameterization at Arica (Poconchile). A slightly better agreement in terms of the slopes with respect to our ground-estimated CODs is explainable, given that the COD values from both parameterizations are smaller than those obtained in the present work, but all of them agree with the behavior noted by Li et al. (2014) for the larger CODs and by Painemal and Zuidema (2011) and King et al. (2013) for the smaller CODs.

4. Conclusions

The visible cloud optical depth for overcast stratocumulus was determined at two typical sites of the Atacama Desert in Northern Chile, the driest region in the world, using solar irradiance broadband measurements in both the total shortwave and UV ranges. The previously measured cloud effective transmittances and solar zenith angles were used to estimate the cloud optical depth with the help of 1D model calculations representing one-layer homogeneous overcast stratocumulus cloudiness.

COD is generally larger at Arica (typical COD ~15) than at Poconchile (typical COD ~11). Both ranges of broadband measurements, ToSI and UVSI, have shown to be reliable to determine the visible cloud optical depth within this frame. The obtained CODs are larger than those estimated by means of two algorithms that parameterize COD as a function of CET, SZA, *g* and *A* (Barnard et al., 2008), and COD as a function of CET, SZA and *A* (Fitzpatrick et al., 2004).

Maximum sensitivity of the ground-retrieved CODs was observed to changes in the cloud droplet effective radius (r_e), surface albedo (*A*) and aerosol optical depth (*AOD*) in both COD_{To} and COD_{UV}, and additionally to changes in the total ozone column (*TOC*) in COD_{UV}. As worst cases, changing their values from the reference $r_e = 8$ μm, $A = 0.10$, $AOD = 0.3$ and $TOC = 270$ DU to $r_e = 5$ μm, $A = 0.0$, $AOD = 0.0$ and $TOC = 320$ DU ($r_e = 11$ μm, $A = 0.20$, $AOD = 0.6$ and $TOC = 220$ DU) implies overestimation (underestimation) of the inferred CODs by about 25% from ToSI and by about 30% from UVSI.

COD values obtained here are similar to those reported from other persistent overcast stratocumulus systems, for instance over the Northeastern Pacific. However, a direct comparison is difficult even with respect to the surrounding stratocumulus over the Southeast Pacific Ocean, as marked gradients in most of related parameters are observed from the coast offshore in the region, product of particular geographical and environmental conditions, natural and anthropogenic, that characterize the continental coastal and inland region and especially the Arica Bight.

A simple rational expression of CET as a function only of COD in the form $CET = 1/(1 + A_e{}^{*}COD)$ allows a phenomenological estimation of the mean (both spectral and regional) broadband surface albedo through the fitting parameter A_e, giving A_e ~ 0.116 for ToSI and A_e ~ 0.065 for UVSI. In turn, this expression provides an immediate solution to the fitting of the ratio CET_{To}/CET_{UV} as a function of COD.

Our ground-estimated CODs at Arica compare reasonably with overpass MODIS satellite-retrieved CODs, simultaneous within a difference of ±5 min, with an increasing difference towards higher CODs attributable in principle to the surface aerosol load characteristic of the region giving larger ground-estimated CODs. On the contrary, for the smaller CODs a slight overestimation is noted of MODIS CODs respect the present ground-estimated CODs, agreeing with reported comparisons against local in situ aircraft COD measurements over this region. This could be caused by the presence of thin high-altitude clouds that are more easily detected by the satellite instruments.

Even though the analyzed database is not too extensive, there are no other previous reports of simultaneous coastal and inland analysis of solar irradiance and cloudiness over this desert western coastal strip of South America, and even less using simultaneous surface measurements of total shortwave solar irradiance and ultraviolet solar irradiance. Several interesting issues appear that encourage going in depth starting from the present results: which processes control the morning course of the COD?, is the known daily subsidence wave, associated with the diurnal heating of the western slope of the Andes mountain chain (Garreaud and Muñoz, 2004; Wood et al., 2009), reflected to some extent in the surface measurements?, given that only days with cloudless afternoons (which are the majority) were selected, do these days present particular dynamical-meteorological-radiative conditions?, what makes different those fewer days whose afternoons remain mostly cloudy?, how is in detail the stratocumulus daily dissipation process from overcast to cloudless conditions?. Then, the diurnal cycle of stratocumulus cloudiness over this region will be a subject of especial attention for future work.

Acknowledgements

This research was funded by Universidad de Tarapacá, Arica, Chile, and the Consejo Nacional de Investigaciones Científicas y Técnicas (CONICET), Agencia Nacional de Promoción Científica y Tecnológica (ANPCyT) and Pontificia Universidad Católica of Argentina. Especial thanks to Rubén Piacentini and to the Instituto de Física de Rosario (CONICET - Universidad Nacional de Rosario), Argentina, for their support to this work, to Christian Retscher and Alexander Cede of the NASA Goddard Space Flight Center for their help to access MODIS data, to Robert Wood of the University of Washington, Seattle, USA, Rene Garreaud of the Universidad de Chile, Santiago, Chile, and to the anonymous reviewers for their helpful comments that contributed to improve the manuscript.

Appendix A. Supplementary data

Supplementary data to this article can be found online at http://dx.doi.org/10.1016/j.atmosres.2016.01.007.

References

Anikine, P.P., Romashova, E.V., Anikine, D.P., 1998. About determination of the cloud optical depth from the data of the Cloud-Radiation-Aerosol Experiments (1994, 1996) at IAPh, Russia. Proc. of the Eighth Atmospheric Radiation Measurement (ARM) Science Team Meeting. U.S. Department of Energy *Washington, D. C.*, Tucson, Arizona, pp. 27–30.

Antón, M., Alados-Arboledas, L., Guerrero-Rascado, J.L., Costa, M.J., Chiu, J.C., Olmo, F.J., 2012. Experimental and modeled UV erythemal irradiance under overcast conditions: the role of cloud optical depth. Atmos. Chem. Phys. 12, 11723–11732. http://dx.doi.org/10.5194/acp-12-11723-2012.

Antón, M., Gil, J.E., Cazorla, A., Fernández-Gálvez, J., Foyo-Moreno, I., Olmo, F.J., Alados-Arboledas, L., 2011. Short-term variability of experimental ultraviolet and total solar irradiance in Southeastern Spain. Atmos. Environ. 45, 4815–4821. http://dx.doi.org/10.1016/j.atmosenv.2011.06.020.

Barker, H.W., Liu, D., 1995. Inferring optical depth of broken clouds from Landsat data. J. Clim. 8, 2620–2630.

Barker, H.W., Curtis, T.J., Leontieva, E., Stamnes, K., 1998. Optical depth of overcast cloud across Canada: estimates based on surface pyranometer and satellite measurements. J. Clim. 11, 2980–2994.

Barker, H.W., Marshak, A., Szyrmer, W., Trishchenko, A., Blanchet, J.-P., Li, Z., 2002. Inference of cloud optical depth from aircraft-based solar radiometric measurements. J. Atmos. Sci. 59, 2093–2111.

Barnard, J.C., Long, C.N., 2004. A simple empirical equation to calculate cloud optical thickness using shortwave broadband measurements. J. Appl. Meteorol. 43, 1057–1066.

Barnard, J.C., Long, C.N., Kassianov, E.I., McFarlane, S.A., Comstock, J.M., Freer, M., McFarquhar, G., 2008. Development and evaluation of a simple algorithm to find cloud optical depth with emphasis on thin ice clouds. Open Atmos. Sci. J. 2, 46–55. http://dx.doi.org/10.2174/1874282300802010046.

Bigorre, S., et al., 2007. Stratus Ocean Reference Station (20°S, 85°W): mooring recovery and deployment cruise, R/V Ronald H. Brown Cruise 06–07, October 9-October 27, 2006. Woods Hole Oceanographic Institution technical report WHOI-2007-01; UOP technical report 2007-01, 154 pp. http://uop.whoi.edu/techdocs/publications.html

Boers, R., 1997. Simultaneous retrievals of cloud optical depth and droplet concentration from solar irradiance and microwave liquid water path. J. Geophys. Res. 102 (D25), 29881–29891.

Boers, R., Van Lammeren, A., Feijt, A., 2000. Accuracy of cloud optical depth retrievals from ground-based pyranometers. J. Atmos. Ocean. Technol. 17, 916–927.

Bretherton, C.S., Uttal, T., Fairall, C.W., Yuter, S.E., Weller, R.A., Baumgardner, D., Comstock, K., Wood, R., Raga, G.B., 2004. The EPIC 2001 stratocumulus study. Bull. Am. Meteorol. Soc. 85, 967–977.

Calbó, J., Pagès, D., González, J., 2005. Empirical studies of cloud effects on UV radiation: a review. Rev. Geophys. 43, RG2002. http://dx.doi.org/10.1029/2004RG000155.

Cede, A., Luccini, E., Nuñez, L., Piacentini, R., Blumthaler, M., 2002. Effects of clouds on erythemal and total irradiance as derived from data of the Argentine network. Geophys. Res. Lett. 29, 24. http://dx.doi.org/10.1029/2002GL015708.

Chand, D., Hegg, D.A., Wood, R., Shaw, G.E., Wallace, D., Covert, D.S., 2010. Source attribution of climatically important aerosol properties measured at Paposo (Chile) during VOCALS. Atmos. Chem. Phys. 10, 10789–10801. http://dx.doi.org/10.5194/acp-10-10789-2010.

Daniel, J.S., Solomon, S., Portmann, R.W., Langford, A.O., Eubank, C.S., Dutton, E.G., Madsen, W., 2002. Cloud liquid water and ice measurements from spectrally resolved near-infrared observations: a new technique. J. Geophys. Res. 107 (D21), 4599. http://dx.doi.org/10.1029/2001JD000688.

Dong, X., Mace, G.G., 2003. Arctic stratus cloud properties and radiative forcing derived from ground-based data collected at Barrow, Alaska. J. Clim. 16, 445–461.

Dong, X., Ackerman, T.P., Clothiaux, E.E., 1998. Parameterizations of the microphysical and shortwave radiative properties of boundary layer stratus from ground-based measurements. J. Geophys. Res. 103 (D24), 31681–31693.

Dong, X., Ackerman, T.P., Clothiaux, E.E., Pilewskie, P., Han, Y., 1997. Microphysical and radiative properties of boundary layer stratiform clouds deduced from ground-based measurements. J. Geophys. Res. 102 (D20), 23829–23843.

Dong, X., Minnis, P., Mace, G.G., Clothiaux, E.E., Liljegren, J.C., 1999. Comparison of stratus cloud microphysical retrievals that utilize radar, microwave radiometer, and pyranometer measurements. Proc. of the Ninth Atmospheric Radiation Measurement (ARM) Science Team Meeting. San Antonio, Texas. U.S. Department of Energy, Washington, D. C.

Dutton, E.G., Michalsky, J.J., Stoffel, T., Forgan, B.W., Hickey, J., Nelson, D.W., Alberta, T.L., Reda, I., 2001. Measurement of broadband diffuse solar irradiance using current commercial instrumentation and a correction for thermal offset errors. J. Atmos. Ocean. Technol. 18, 297–314.

Eck, T.F., et al., 2012. Fog- and cloud-induced aerosol modification observed by the aerosol robotic network (AERONET). J. Geophys. Res. 117, D07206. http://dx.doi.org/10.1029/2011JD016839.

Evans, W., Puckrin, E., 1996. Near-infrared spectral measurements of liquid water absorption by clouds. Geophys. Res. Lett. 23 (15), 1941–1944. http://dx.doi.org/10.1029/96GL01473.

Fitzpatrick, M.F., Warren, S.G., 2005. Transmission of solar radiation by clouds over snow and ice surfaces. Part II: cloud optical depth and shortwave radiative forcing from pyranometer measurements in the Southern Ocean. J. Clim. 18, 4637–4648.

Fitzpatrick, M.F., Brandt, R.E., Warren, S.G., 2004. Transmission of solar radiation by clouds over snow and ice surfaces: A parameterization in terms of optical depth, solar zenith angle, and surface albedo. J. Clim. 17, 266–275.

Fu, Q., Liou, K.N., 1992. On the correlated k-distribution method for radiative transfer in nonhomogenous atmospheres. J. Atmos. Sci. 49, 2139–2156.

Fu, Q., Liou, K.N., 1993. Parameterization of the radiative properties of cirrus clouds. J. Atmos. Sci. 50, 2008–2025.

Garreaud, R.D., Muñoz, R., 2004. The diurnal cycle in circulation and cloudiness over the subtropical Southeast Pacific: A modeling study. J. Clim. 17, 1699–1710.

Garreaud, R.D., Wallace, J.M., 1997. The diurnal march of convective cloudiness over the Americas. Mon. Weather Rev. 125, 3157–3171.

Garreaud, R.D., Rutllant, J.A., Muñoz, R.C., Rahn, D.A., Ramos, M., Figueroa, D., 2011. VOCALS-CUpEx: the Chilean upwelling experiment. Atmos. Chem. Phys. 11, 2015–2029. http://dx.doi.org/10.5194/acp-11-2015-2011.

Harrison, R.G., Chalmers, N., Hogan, R.J., 2008. Retrospective cloud determinations from surface solar radiation measurements. Atmos. Res. 90, 54–62.

Harshvardhan, G.G., Green, R.N., Qu, Z., Nakajima, T.Y., 2004. Remotely sensed microphysical and thermodynamic properties of nonuniform water cloud fields. J. Atmos. Sci. 61 (21), 2574–2587.

Hu, Y.-X., Stamnes, K., 1993. An accurate parameterization of the radiative properties of water clouds suitable for use in climate models. J. Clim. 6 (4), 728–742.

Huneeus, N., Gallardo, L., Rutllant, J.A., 2006. Offshore transport episodes of anthropogenic sulfur in Northern Chile: potential impact on the stratocumulus cloud deck. Geophys. Res. Lett. 33, L19819. http://dx.doi.org/10.1029/2006GL026921.

King, M.D., Platnick, S., Yang, P., Arnold, G.T., Gray, M.A., Riedi, J.C., Ackerman, S.A., Liou, K.N., 2004. Remote sensing of liquid water and ice cloud optical thickness and effective radius in the arctic: application of airborne multispectral MAS data. J. Atmos. Ocean. Technol. 21, 857–875.

King, M.D., Radke, L.F., Hobbs, P.V., 1990. Determination of the spectral absorption of solar radiation by marine stratocumulus clouds from airborne measurements within clouds. J. Atmos. Sci. 47, 894–907.

King, M.D., Tsay, S-Ch., Platnick, S., Wang, M., Liou, K.N., 1998. Cloud retrieval algorithms for MODIS: optical thickness, effective particle radius, and thermodynamic phase. MODIS Algorithm Theoretical Basis Document No. ATBD-MOD-05 MOD06 – Cloud product.

King, N.J., Bower, K.N., Crosier, J., Crawford, I., 2013. Evaluating MODIS cloud retrievals with in situ observations from VOCALS-REx. Atmos. Chem. Phys. 13, 191–209. http://dx.doi.org/10.5194/acp-13-191-2013.

Kokhanovsky, A.A., 2003. The influence of horizontal inhomogeneity on radiative characteristics of clouds: an asymptotic case study. IEEE Trans. Geosci. Remote Sens. 41 (4), 817–825.

Kollias, P., Fairall, C.W., Zuidema, P., Tomlinson, J., Wick, G.A., 2004. Observations of marine stratocumulus in SE Pacific during the PACS 2003 cruise. Geophys. Res. Lett. 31, L22110.

Kuo, K.-S., Welch, R.M., Gao, B.C., Goetz, A.F., 1990. Cloud identification and optical thickness retrieval using AVIRIS data. Proc. of the Second Airborne Visible/Infrared Imaging Spectrometer (AVIRIS) Workshop. JPL Publication (90–54).

Leontyeva, E., Stamnes, K., 1994. Estimations of cloud optical thickness from ground-based measurements of incoming solar radiation in the Arctic. J. Clim. 7, 566–578.

Li, Z., Garand, L., 1994. Estimation of surface albedo from space: A parameterization for global application. J. Geophys. Res. 99 (D4), 8335–8350.

Li, Z., Trishchenko, A.P., Chang, F.-L., Barker, H.W., Sun, W.B., 1999. Consistency check of cloud optical properties derived from satellite and surface observations. Proc. of the Ninth ARM Science Team Meeting, San Antonio, Texas. U.S. Department of Energy, Washington, D. C.

Li, Z., Zhao, F., Liu, J., Jiang, M., Zhao, C., Cribb, M., 2014. Opposite effects of absorbing aerosols on the retrievals of cloud optical depth from spaceborne and ground-based measurements. J. Geophys. Res. Atmos. 119. http://dx.doi.org/10.1002/2013JD021053.

Loeb, N.G., Coakley Jr., J.A., 1998. Inference of marine stratus cloud optical depths from satellite measurements: does 1D theory apply? J. Clim. 11, 215–232.

Long, C.N., Gaustad, K.L., Younkin, K., Augustine, J.A., 2003. An improved daylight correction for IR loss in ARM diffuse SW measurements. Proc. of the Thirteenth ARM Science Team Meeting. Broomfield, Colorado U.S. Department of Energy, *Washington, D. C.*

Luccini, E., Rivas, M., Rojas, E., Canziani, P., 2011. Cloud effective transmittance at two sites of the Atacama Desert, Chile. J. Geophys. Res. 116, D20205. http://dx.doi.org/10.1029/2011JD015905.

Marshak, A., Knyazikhin, Y., Davis, A.B., Wiscombe, W.J., Pilewskie, P., 2000. Cloud-vegetation interaction: use of normalized difference cloud index for estimation of cloud optical thickness. Geophys. Res. Lett. 27 (12), 1695–1698. http://dx.doi.org/10.1029/1999GL010993.

Matamoros, S., González, J.-A., Calbó, J., 2011. A simple method to retrieve cloud properties from atmospheric transmittance and liquid water column measurements. J. Appl. Meteorol. Climatol. 50, 283–295. http://dx.doi.org/10.1175/2010JAMC2394.1.

Mateos, D., Antón, M., Valenzuela, A., Cazorla, A., Olmo, F.J., Alados-Arboledas, L., 2014. Efficiency of clouds on shortwave radiation using experimental data. Appl. Energy 113, 1216–1219. http://dx.doi.org/10.1016/j.apenergy.2013.08.060.

McKinlay, A.F., Diffey, B.L., 1987. A reference action spectra for ultraviolet introduced erythema in human skin. In: Passchier, W.R., Bosnajakovich, B.M.F. (Eds.), Human Exposure to Ultraviolet Radiation: Risks and Regulations. Elsevier, New York, pp. 83–87.

Mechoso, C., Wood, R., Bretherton, C.S., Clarke, A., Coe, H., Fairall, C., Farrar, J.T., Feingold, G., Garreaud, R., Grados, C., McWilliams, J., de Szoeke, S., Yuter, S., Zuidema, P., 2014. Ocean-cloud-atmosphere-land interactions in the Southeast Pacific: the VOCALS program. Bull. Am. Meteorol. Soc. 95 (3), 357–375. http://dx.doi.org/10.1175/BAMS-D-11-00246.1.

Min, Q., Harrison, L.C., 1996. Cloud properties derived from surface MFRSR measurements and comparison with GOES results at the ARM SGP site. Geophys. Res. Lett. 23 (13), 1641–1644.

Min, Q., Harrison, L.C., 1998. Comparison of model-predicted total shortwave with measurements under overcast cloud conditions. Proc. of the Eighth Atmospheric Radiation Measurement (ARM) Science Team Meeting. U.S. Department of Energy, *Washington, D. C.*, Tucson, Arizona.

Min, Q., Duan, M., Marchand, R., 2003. Validation of surface retrieved cloud optical properties with in situ measurements at the atmospheric radiation measurement program (ARM) South Great Plains site. J. Geophys. Res. 108 (D17), 4547. http://dx.doi.org/10.1029/2003JD003385.

Min, Q., Joseph, E., Duan, M., 2004. Retrievals of thin cloud optical depth form a multifilter rotating shadowband radiometer. J. Geophys. Res. 109, D02201. http://dx.doi.org/10.1029/2003JD003964.

Nakajima, T., King, M.D., Spinhirne, J.D., Radke, L.F., 1991. Determination of the optical thickness and effective particle radius of clouds from reflected solar radiation measurements. Part II: marine stratocumulus observations. J. Atmos. Sci. 48, 728–751. http://dx.doi.org/10.1175/1520-0469(1991)048<0728:DOTOTA>2.0.CO;2.

Otero, L., Ristori, P., Holben, B., Quel, E., 2006. Aerosol optical thickness at ten AERONET/NASA stations during 2002. Opt. Pura Apl. 39, 355–364.

Painemal, D., Zuidema, P., 2010. Microphysical variability in Southeast Pacific stratocumulus clouds: synoptic conditions and radiative response. Atmos. Chem. Phys. 10, 6255–6269. http://dx.doi.org/10.5194/acp-10-6255-2010.

Painemal, D., Zuidema, P., 2011. Assessment of MODIS cloud effective radius and optical thickness retrievals over the Southeast Pacific with VOCALS-REx in situ measurements. J. Geophys. Res. 116, D24206. http://dx.doi.org/10.1029/2011JD016155.

Platnick, S., King, M.D., Ackerman, S.A., Menzel, W.P., Baum, B.A., Riedl, C., Frey, R.A., 2003. The MODIS cloud products: algorithms and examples from Terra. IEEE Trans. Geosci. Remote Sens. Aqua Spec. Issue 41, 459–473.

Qiu, J., 2006. Cloud optical thickness retrievals from ground-based pyranometer measurements. J. Geophys. Res. 111, D22206. http://dx.doi.org/10.1029/2005JD006792.

Rawlins, F., Foot, J.S., 1990. Remotely sensed measurements of stratocumulus properties during FIRE using the C130 aircraft multi-channel radiometer. J. Atmos. Sci. 47 (21), 2488–2504.

Rose, F.G., Charlock, T.P., 2002. New Fu-Liou code tested with ARM Raman Lidar and CERES in pre-CALIPSO exercise. Extended abstract for 11th Conference on Atmospheric Radiation (AMS). Ogden, Utah.

Rossow, W.B., Schiffer, R.A., 1991. ISCCP cloud data products. Bull. Am. Meteorol. Soc. 72, 2–20.

Rozwadowska, A., 2004a. Optical thickness of stratiform clouds over the Baltic inferred from on-board irradiance measurements. Atmos. Res. 72, 129–147.

Rozwadowska, A., 2004b. Uncertainty in stratiform cloud optical thickness inferred from pyranometer measurements at the sea surface. Oceanology 46, 155–174.

Rutllant, J.A., Muñoz, R.C., Garreaud, R.D., 2013. Meteorological observations on the northern Chilean coast during VOCALS-REx. Atmos. Chem. Phys. 13, 3409–3422. http://dx.doi.org/10.5194/acp-13-3409-2013.

Serpetzoglou, E., Albrecht, B.A., Kollias, P., Fairall, C.W., 2008. Boundary layer, cloud, and drizzle variability in the Southeast Pacific stratocumulus regime. J. Clim. 21, 6191–6214. http://dx.doi.org/10.1175/2008JCLI2186.1.

Serrano, D., Marín, M.J., Núñez, M., Gandía, S., Utrillas, M.P., Martínez-Lozano, J.A., 2015b. Relationship between the effective cloud optical depth and different atmospheric transmission factors. Atmos. Res. 160, 50–58. http://dx.doi.org/10.1016/j.atmosres.2015.03.004.

Serrano, D., Marín, M.J., Núñez, M., Utrillas, M.P., Gandía, S., Martínez-Lozano, J.A., 2015a. Wavelength dependence of the effective cloud optical depth. J. Atmos. Sol. Terr. Phys. 130-131, 14–22. http://dx.doi.org/10.1016/j.jastp.2015.05.001.

Serrano, D., Marín, M.J., Utrillas, M.P., Martínez-Lozano, J.A., Núñez, M., Gómez-Amo, J.L., 2013. Estimation of cloud optical depth for low clouds from UV erythemal irradiance. AIP Conf. Proc. 1531, 895–898. http://dx.doi.org/10.1063/1.4804915.

Serrano, D., Núñez, M., Utrillas, M.P., Marín, M.J., Marcos, C., Martínez-Lozano, J.A., 2014. Effective cloud optical depth for overcast conditions determined with a UV radiometers. Int. J. Climatol. 34, 3939–3952. http://dx.doi.org/10.1002/joc.3953.

Su, W., Charlock, T.P., Rose, F.G., 2005. Deriving surface ultraviolet radiation from CERES surface and atmospheric radiation budget: methodology. J. Geophys. Res. 110, D14209. http://dx.doi.org/10.1029/2005JD005794.

Szczodrak, M., Austin, P.H., Krummel, P.B., 2001. Variability of optical depth and effective radius in marine stratocumulus clouds. J. Atmos. Sci. 58, 2912–2926. http://dx.doi.org/10.1175/1520-0469(2001)058<2912:VOODAE>2.0.CO;2.

Twohy, C.H., Anderson, J.R., Toohey, D.W., Andrejczuk, M., Adams, A., Lytle, M., George, R.C., Wood, R., Saide, P., Spak, S., Zuidema, P., Leon, D., 2013. Impacts of aerosol particles on the microphysical and radiative properties of stratocumulus clouds over the Southeast Pacific Ocean. Atmos. Chem. Phys. 13, 2541–2562. http://dx.doi.org/10.5194/acp-13-2541-2013.

Varotsos, C.A., Melnikova, I.N., Cracknell, A.P., Tzanis, C., Vasilyev, A.V., 2014. New spectral functions of the near-ground albedo derived from aircraft diffraction spectrometer observations. Atmos. Chem. Phys. 14, 6953–6965. http://dx.doi.org/10.5194/acp-14-6953-2014.

Vignola, F., Long, C.N., Reda, I., 2007. Evaluation of methods to correct for IR loss in Eppley PSP diffuse measurements. In: Myers, D.R. (Ed.), Optical Modeling and Measurements for Solar Energy Systems. Proc. SPIE 6652. http://dx.doi.org/10.1117/12.734474.

Wood, R., 2012. Stratocumulus clouds. Mon. Weather Rev. 140, 2373–2423.

Wood, R., Köhler, M., Bennartz, R., O'Dell, C., 2009. The diurnal cycle of surface divergence over the global oceans. Quart. J. Roy. Meteorol. Soc. 135, 1484–1493. http://dx.doi.org/10.1002/qj.451.

Wood, R., et al., 2011. The VAMOS Ocean-cloud-atmosphere-land study regional experiment (VOCALS-REx): goals, platforms, and field operations. Atmos. Chem. Phys. 11, 627–654. http://dx.doi.org/10.5194/acp-11-627-2011.

Yin, B., Min, Q., Duan, M., Bartholomew, M.J., Vogelmann, A.M., Turner, D.D., 2011. Retrievals of cloud optical depth and effective radius from thin-cloud rotating shadowband radiometer measurements. J. Geophys. Res. 116 (D23208). http://dx.doi.org/10.1029/2011JD016192.

Younkin, K., Long, C.N., 2003. Improved correction of IR loss in diffuse shortwave measurements: an ARM value added product. (ARM TR-009) http://www.arm.gov/publications/techreports.stm.

Zender, C.S., Talamantes, J., 2006. Solar absorption by Mie resonances in cloud droplets. J. Quant. Spectrosc. Radiat. Transf. 98 (1), 122–129. http://dx.doi.org/10.1016/j.jqsrt.2005.05.084.

Zhang, G.J., Vogelmann, A.M., Jensen, M.P., Collins, W.D., Luke, E.P., 2010. Relating satellite-observed cloud properties from MODIS to meteorological conditions for marine boundary layer clouds. J. Clim. 23, 1374–1391. http://dx.doi.org/10.1175/2009JCLI2897.1.

Ziemke, J.R., Chandra, S., Labow, G.J., Bhartia, P.K., Froidevaux, L., Witte, J.C., 2011. A global climatology of tropospheric and stratospheric ozone derived from Aura OMI and MLS measurements. Atmos. Chem. Phys. 11, 9237–9251. http://dx.doi.org/10.5194/acp-11-9237-2011.

Zinner, T., Mayer, B., 2006. Remote sensing of stratocumulus clouds: uncertainties and biases due to inhomogeneity. J. Geophys. Res. 111, D14209. http://dx.doi.org/10.1029/2005JD006955.

Zuidema, P., Painemal, D., deSzoeke, S., Fairall, C., 2009. Stratocumulus cloud-top height estimates and their climatic implications. J. Clim. 22, 4652–4666. http://dx.doi.org/10.1175/2009JCLI2708.1.